ELSEVIER

Catalysis Today 64 (2001) 163–177

CATALYSIS TODAY

www.elsevier.com/locate/cattod

Kinetics of carbon oxide evolution in temperature-programmed oxidation of carbonaceous laydown deposited on wet oxidation catalysts

F. Larachi [a,*], K. Belkacemi [b], S. Hamoudi [a], A. Sayari [a]

[a] *Department of Chemical Engineering and CERPIC, Laval University, Laval, Que., Canada G1K 7P4*
[b] *Department of Food Science and Nutrition, Laval University, Laval, Que., Canada G1K 7P4*

Abstract

The combustion kinetics of coke laydown on wet oxidation catalysts was studied by means of temperature-programmed oxidation and mass spectrometry within the temperature range (30–600°C). The coke deposits were formed over three different catalysts 1 wt.% Pt/Al_2O_3, MnO_2/CeO_2 and 1 wt.% $Pt–MnO_2/CeO_2$ during phenol deep oxidation in a three-phase slurry reactor at various reaction conditions (exposure time, temperature, oxygen pressure, catalyst loading). The carbon oxides, oxygen and water fluxes arising from the combustion of the carbonaceous deposits in a 5% O_2/He mixture, were continuously monitored. In all cases, unimodal quasi-Gaussian distributions were obtained for CO_2 while no CO was detected. These evolutions were successfully described by a modified "fractal power-law" grain model. The coke-dependence of the carbon dioxide profiles was related to the fractal dimension of the catalyst surface and to the oxygen partial order during coke burn-off. The corresponding change in O_2 partial order was ascribed to competition between three steps in the combustion mechanism: non-dissociative O_2 chemisorption, interaction of oxygen with undissociated dioxygen bearing surface species, physical desorption of the complex oxide as carbon dioxide.

Keywords: Wet oxidation; Catalyst deactivation; "Coke" morphology; "Coke" burn-off kinetics

1. Introduction

Several abiotic processes are known to be efficient in transforming water-dissolved biorefractory contaminants into environmentally innocuous entities. Among them, catalytic wet oxidation (CWO) is gaining in popularity, especially for wastewaters having pollutant loads intermediate between those suitable for conventional biotreatment and for incineration processes. Highly active *solid* catalysts, combined with pressurized O_2 under mild temperature/pressure, are able to trigger the oxidation of pollutants dissolved in wastewaters, eventually to a deeper level of complete mineralization [1].

Important emphasis is being put nowadays on finding efficient CWO solid catalysts able to accomplish oxidative destruction of aqueous pollutants under *acceptably* moderate conditions. This endeavor is largely dictated by the fact that there are virtually no immediate profits from obtaining "clean" but "zero-added-value" treated waters, besides the sole safeguard of the environment. Whereas compliance with the regulation in terms of discharge tolerances is always accompanied by extra costs.

Integration of CWO multiphase reactors into viable water treatment units must take into account one key

* Corresponding author. Tel.: +1-418-656-3566; fax: +1-418-656-5993.
E-mail address: flarachi@gch.ulaval.ca (F. Larachi).

0920-5861/01/$ – see front matter
PII: S0920-5861(00)00521-6

aspect of solid catalysts, that is catalyst regeneration. Coke formation leading to catalyst deactivation is an inevitable *parasitic* chemical reaction that occurs concomitantly with the pollutant mineralization [2–5]. As the carbonaceous overlayer deactivates the catalyst, "coke" burn-off is explored as an option for activity restoration.

The CWO deposits dealt within this work share certain similarities with the carbonaceous deposits formed by the reaction of hydrocarbons in the presence of H_2 over cracking and reforming catalysts [6–9]. However, if the coke formed during hydrocarbon conversion has been the subject of thorough investigations over several decades, literature pertinent to CWO "coke" is virtually *non-existent*. There is therefore a strong need to bring new knowledge and to provide some insights into the surface chemistry of the carbonaceous materials building up over wet oxidation catalysts. Furthermore, from the perspective of catalytic reactor engineering, these informations are essential to successfully design long-lasting wastewater treatment units able to overcome the unavoidable catalyst coke laydown deactivation, but also for the optimal sizing/rating of the regeneration units for activity rendition of the spent CWO catalysts.

The objectives of this work are twofold. First, the combustion kinetics, in the temperature-programmed oxidation mode (TPO), of carbonaceous deposits on spent Pt/Al_2O_3, MnO_2/CeO_2 and $Pt–MnO_2/CeO_2$ catalysts used for CWO of phenolic aqueous solutions are studied and qualitatively discussed. Second, a mechanistic pathway and a phenomenological kinetic model are proposed for the description of the TPO of CWO coke combustion.

2. Brief survey of coke burning modeling approaches

In order to optimize the catalyst regeneration, understanding of the kinetics of the evolving gaseous products (CO, CO_2, and H_2O) formed by combustion of the deposits is needed. Depending on the CWO history and conditions, several physico-chemical phenomena can affect the combustion of the coke deposited on the catalyst surface. These include surface area modification, change in effective O_2 diffusivity in the pores of the coked matrix, interactions with native impurities inducing catalytic or inhibiting effects, etc. Coke may also be altered by thermal rearrangements, pyrolysis, changes in functional groups (for example, hydrogen loss during coke combustion), etc.

A rigorous, and perhaps utopian, treatment of the combustion kinetics must enmesh all of these features to form a detailed knowledge and understanding for such particular CWO reactions. Usually, comprehensive kinetic models for combustion of carbonaceous deposits including such a level of sophistication are cumbersome and mathematically difficult to handle in practical contexts.

Rather, alternative simplified approaches were proposed. Early works proposed diffusion-control or shrinking-core models in the case of single-pellet regeneration [9–16]. Other works used global kinetics and applied power-law rate expressions wherein burn-off data were fitted with a first-order reaction model with respect to coke and an order varying in the range (0–1) for oxygen pressure [17–23]. The coke burn-off profiles were also approached (semi-)mechanistically for carbon speciation using peak synthesis/decomposition of complex TPO spectra into several single-step narrow peaks [7,24–26]. Each carbon peak was ascribed to the presence of a type of carbon that burns following its own global pseudo-kinetic power-law expression.

3. Experimental section

3.1. Coke deposition

The equipment and techniques used to form the carbonaceous deposits, or "coke", on the catalysts were described in detail elsewhere [27,28]. Briefly, the phenol "coking" tests were performed in a stainless steel high pressure autoclave batch slurry reactor (Model 4842, Parr Instrument) shown in Fig. 1a. Aqueous phenol solutions, typically 100 ml, underwent CWO over 1 wt.% Pt/Al_2O_3 (Aldrich), MnO_2/CeO_2 and 1 wt.% $Pt–MnO_2/CeO_2$ catalysts. In each CWO run, 100–500 mg of catalyst was coked in an atmosphere of oxygen (0.5–1.5 MPa) at set temperatures in the range 80–175°C and using 0.013–1 g phenol in water. The corresponding O_2-to-phenol stoichiometric ratios were in-between 2.5 and 108.

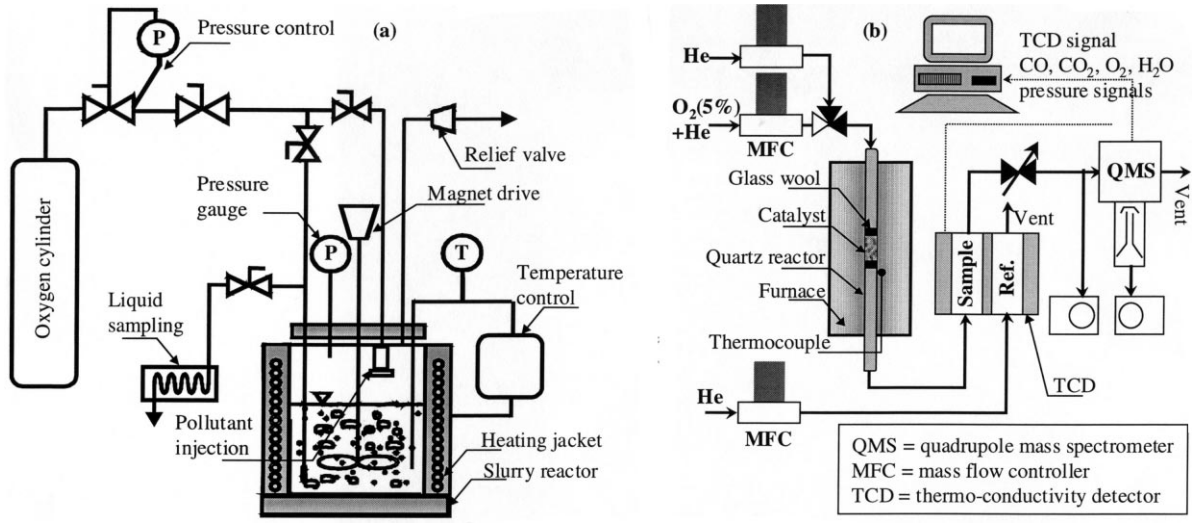

Fig. 1. Layouts of the experimental facilities used in the: (a) phenol coking tests in a three-phase slurry reactor; (b) temperature programmed oxidation of the spent catalyst.

Fresh 1 wt.% Pt/alumina catalyst was initially calcined for 16 h up to 425°C according to the procedure of Ref. [29]. Fresh MnO_2/CeO_2 and 1 wt.% Pt–MnO_2/CeO_2 catalysts, synthesized in our laboratory, were calcined at 350°C for 3 h as described in Ref. [4]. The catalysts were then contacted for up to 4 h with the phenolic solutions in the CWO slurry reactor. For measurement of the activity loss profiles versus time, several CWO batches were run under exactly identical conditions, but were quenched in order of increasing oxidation reaction times. Hence, subsequent to a reaction quenching, the (partially) deactivated catalyst was withdrawn from the slurry reactor regularly every 5 min, washed and air-dried. For each operating condition, the spent catalyst was divided into 50–100 mg batches for TPO–MS studies, nitrogen BET surface area, SEM, XPS and elemental analysis determinations.

3.2. TPO–MS facility

The TPO–MS experimental facility is drawn schematically in Fig. 1b. It consisted of a $\frac{1}{4}$ in. i.d. flow-through U-shaped tubular quartz microreactor placed in an electrically heated and temperature program-controlled ceramic furnace. At about mid-height deep in the furnace, 50–100 mg of spent catalyst was placed inside the reactor and sandwiched in-between two glass wool plugs. Such small amounts of catalyst are required to prevent large temperature fluctuations in the gas stream due to the exothermicity of combustion and excessive peak broadening due to multiple readsorption. Temperature was measured by a thermocouple positioned flush to the microreactor wall, and pressure by a pressure gauge located at the reactor outlet.

Each batch of spent catalyst was first exposed to flowing helium (30 ml/min) while starting a linear temperature program at a heating rate of 10°C/min from ambient to 120°C, where it was kept for 20 min before cooling down to room temperature. Such a systematic treatment allowed removal of physisorbed water from the catalyst sample without thermally modifying the nature of the deposited coke [27]. Subsequently, the catalyst was heated up to 650°C at 8°C/min under a controlled flow of 5% oxygen diluted in helium passing through the catalyst bed to burn-off the carbonaceous deposit. The volumetric gas flow rate was 30 ml/min.

Oxygen uptake, O_2, CO, CO_2 and H_2O fluxes evolving in the gas phase downstream of the microreactor were continuously detected by a thermal conductivity detector (TCD) and by mass spectrometry using a transpector quadrupole (Leybold Inficon). A fraction

of the off gases flowing downstream of the quartz reactor was diverted into a multiple-stage pressure reduction system. This system consisted of a metering valve that allowed a controlled bleeding of the "shunted" off-gases into the mass spectrometer. The latter was pumped by means of mechanical pumps and a turbo-molecular pump operating at a vacuum pressure near 10^{-6} Torr. The TCD and MS signals were recorded on a personal computer interfaced to the instruments via data acquisition boards. The sampling period of the signals was 5 s.

The mass spectrometry signals corresponding to the four gas components measured under vacuum (CO, CO_2, O_2, H_2O) were converted into production/consumption rates in the conditions of the microreactor outlet:

$$\text{Rate}[\mu\text{mol}/(\text{g cat.}\,^\circ\text{C})] = \frac{J}{S}\frac{P_\text{o}}{P_\text{d}}\frac{Q}{RT}\frac{10^6}{\beta w_\text{cat}} \quad (1)$$

The units for these evolution rates were determined from:

- the electrical current, J (in mA), measured for each species, i.e., O_2, CO, etc.;
- the tabulated mass spectrometer sensitivity factor, S, in mA/atm, for each species;
- the MS-side total pressure, P_d in atm;
- the microreactor-side total pressure P_o in atm, determined to be 1.2 atm for all the runs;
- the mass of catalyst, w_cat in g;
- the combustion temperature, T in °C;
- the heating rate, β in °C/min;
- the microreactor flow-through volumetric rate, Q in l/min.

For kinetic modeling, the carbon oxide rates were expressed as carbon conversion rates:

$$\frac{\mathrm{d}X}{\mathrm{d}T} = \frac{J}{S}\frac{P_\text{o}}{P_\text{d}}\frac{Q}{RT}\frac{10^6}{\beta[C]_\text{o} w_\text{cat}} \quad (2)$$

Here R is the ideal gas constant and $[C]_\text{o}$ the concentration, in μmol/(g cat.), of total carbon measured using a Carlo Erba CHN analyzer.

The average particle size for fresh and spent catalysts was ca. 70 μm and the high molecular diffusivity of O_2 in He ensured that the combustion rates were not mass-transfer controlled. Moreover, assuming a heat of combustion of ca. 30 kJ/g [30] led to a temperature difference between the catalyst surface and the gas bulk less than 0.01 K concluding to the non-influence of heat-transfer limitations. All gases were supplied by Praxair (Québec) and the gas flow rates were stabilized and measured by Brooks mass-flow controllers.

3.3. Analytical methods

Texture and morphology of the spent and fresh catalysts were examined using a 515 Philips scanning electron microscope (SEM) at different scales/magnifications. The oxidation states of Pt, Mn and Ce over the fresh and spent catalysts were determined by X-ray photoelectron spectroscopy (XPS) using a V.G. Scientific Escalab Mark II system. The BET specific surface areas were obtained using N_2 physical adsorption at 77 K on a Micromeritics Gemini 2360 sorption instrument. Fractal surface characterization of the catalysts was also attempted by using a modified Brunauer–Emmett–Teller (BET) equation of adsorption isotherms accounting for surface roughness and fractality [31]. The time evolution of the carbon content in the carbonaceous deposits was followed by CHN elemental analysis (Carlo Erba, Model 1106). Similarly, the residual phenol concentration and total organic carbon (TOC) were monitored as a function of reaction time by means of a gas chromatograph (HP5890 series II plus) coupled with a mass selective spectrometer (MSD Model HP5972), and a combustion/non-dispersive infrared gas analyzer (Shimadzu 5050 TOC analyzer), respectively.

4. Experimental results

4.1. Adsorption isotherms and SEM images

Fig. 2a–c shows the adsorption isotherms obtained for virgin and spent catalysts in the case of MnO_2/CeO_2, Pt–MnO_2/CeO_2 and Pt/Al_2O_3, respectively. The CWO reaction conditions and the resulting BET surface areas are also listed in the figures. A notable reduction in surface area occurred with increasing the reaction time of catalyst-mediated phenol CWO. The surface area decreased by 11, 6 and 14%, for MnO_2/CeO_2, Pt–MnO_2/CeO_2 and Pt/Al_2O_3, catalysts, respectively.

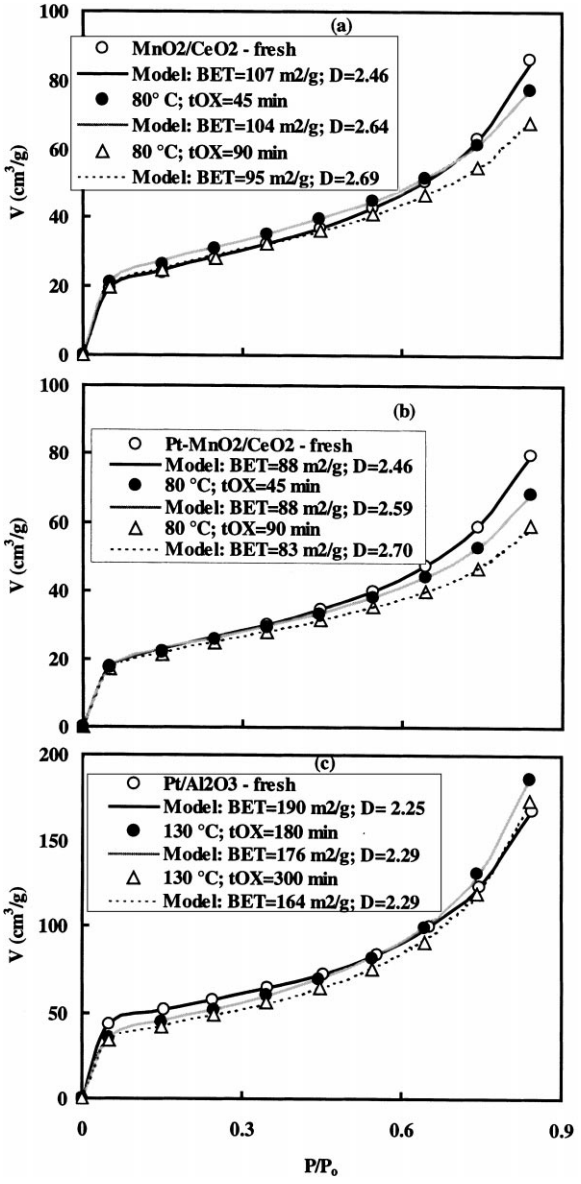

Fig. 2. Adsorption isotherms, BET surface areas and fractal dimensions for fresh and spent: (a) MnO_2/CO_2; (b) Pt–MnO_2/CO_2; (c) Pt–Al_2O_3 catalysts.

The evolution with CWO conditions of the catalyst surface roughness was quantified using the modified "fractal isotherm BET model" developed by Aguerre et al. [31]. Predictions by fitting this model to adsorbed nitrogen volume as a function of reduced pressure are shown in Fig. 2a–c along with the corresponding surface fractal dimension, *D*. Without going through details, this surface fractal dimension can be thought of as a measure of the *irregularity* of the surface delineated by the boundary of the grains composing the catalyst powder. The smoother their surface, the closer the *D* to a value of 2, the more irregular the surface the closer it is to a value of 3.

The fractal dimensions increase correlatively with the decrease in BET surface area suggesting that the "coked" catalyst surfaces became increasingly irregular and the relative sorption capacity of N_2 diminished while coke was being deposited. This may also be confirmed by direct inspection of the SEM photographs in Fig. 3 which show that the lower surface areas are the result of formation of larger size grains, while the greater fractal dimension comes from the increased disparities of the solid surfaces. Hence, the adsorption isotherms of the catalyst surfaces are affected in various extents by the different wet oxidation conditions. The fractal dimension mostly affects the shape of the adsorption isotherms in the upward curvature at high P/P_o ratios. The relative sorption capacity drops there as a consequence of a depletion in the pores population. Whereas for the region at low P/P_o, the fractal BET curves measured in our conditions appeared to be fairly insensitive to the fractal character of the catalyst surface.

As will be shown later, knowledge of the surface fractal dimension will be useful in the derivation of a burn-off kinetic model.

4.2. TPO–MS peak characterization

The TPO–MS profiles of evolved CO_2, H_2O and O_2 (in μmol/(g cat. °C)) are shown in Fig. 4 for the MnO_2/CeO_2 and Pt–MnO_2/CeO_2 catalysts coked at 80°C for 15 min, and for the Pt/Al_2O_3 catalyst contacted for 60 min at 175°C with phenol. In all three cases, no CO was detected. The coke formed on both composite oxide catalysts was very reactive and burnt at much lower temperatures than the deposit over the Pt/alumina catalyst.

4.2.1. Carbon dioxide rate profiles

The CO_2 evolution profiles for the ceria-containing catalysts (Fig. 4a and b) exhibited quasi-symmetrical Gaussian *single peaks*. These "low-temperature"

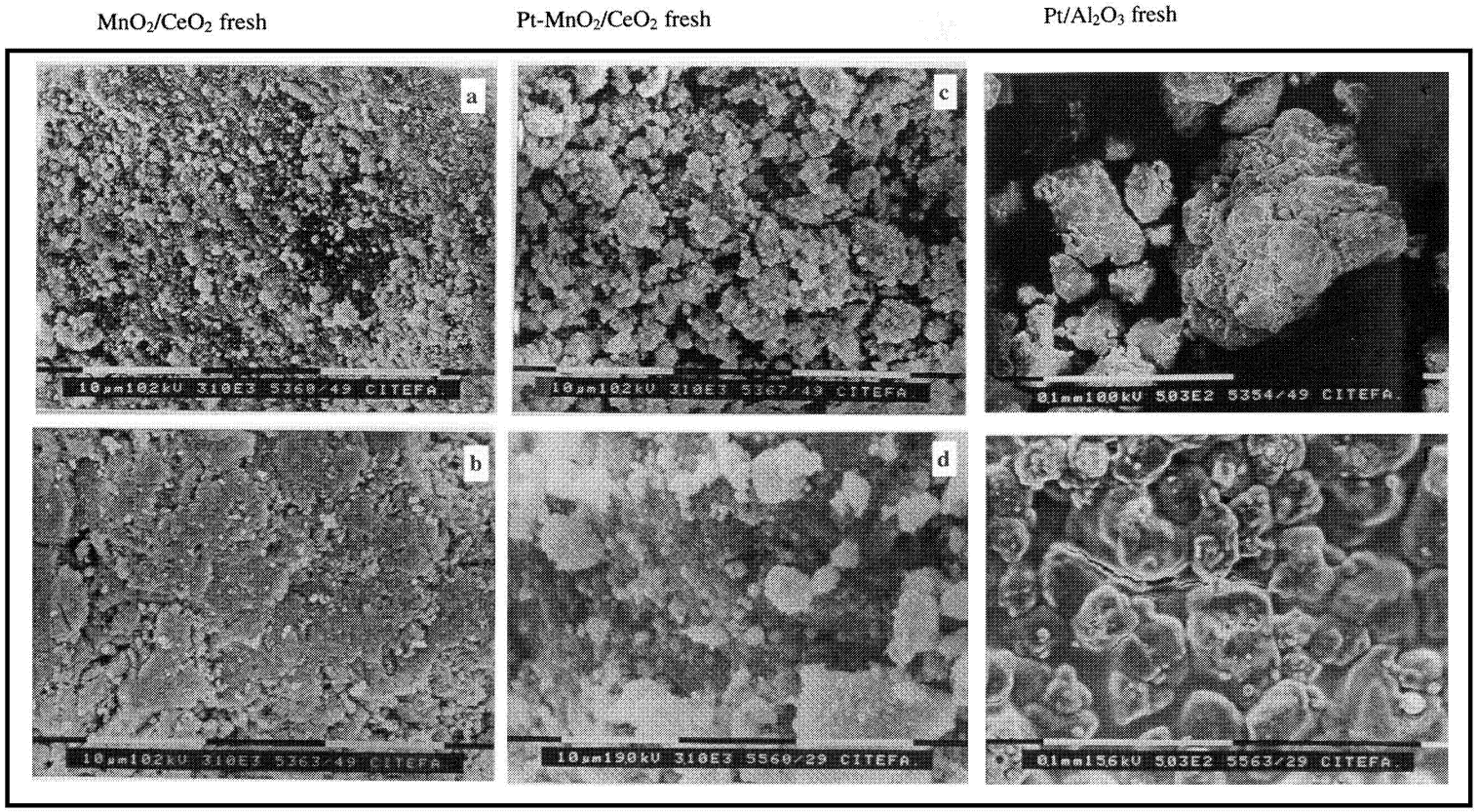

Fig. 3. SEM photographs showing, respectively, fresh and spent: (a) and (b) MnO_2/CO_2; (c) and (d) Pt–MnO_2/CO_2; (e) and (f) Pt–Al_2O_3 catalysts.

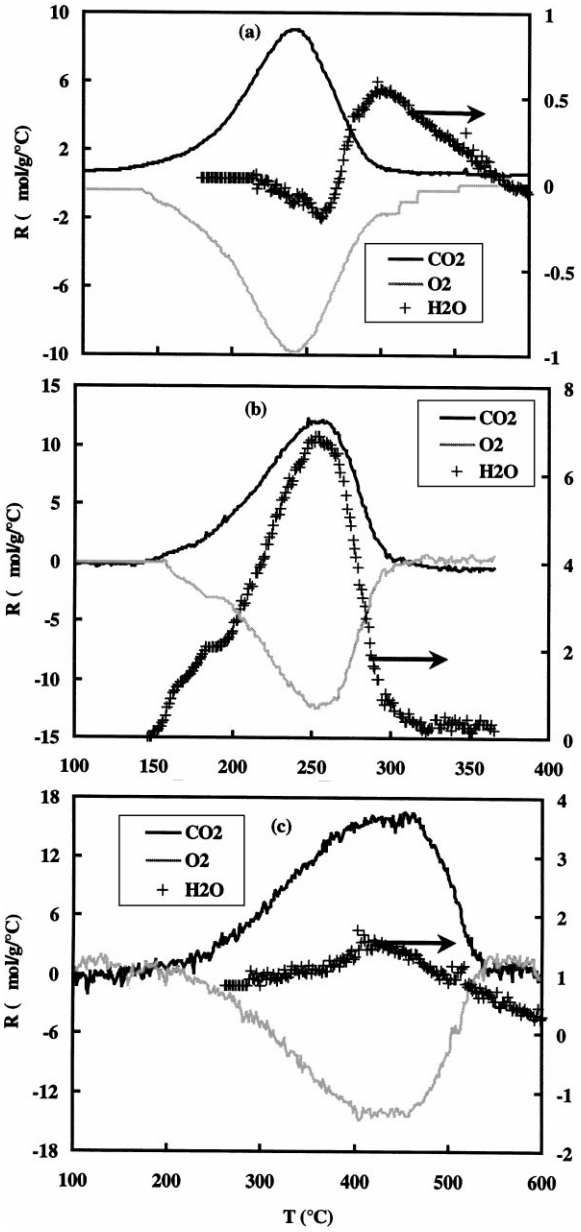

Fig. 4. Experimental evolution rates of CO_2, O_2, and H_2O during TPO in 5% O_2–He mixture at heating rate of 8°C/min of: (a) MnO_2/CO_2; (b) Pt–MnO_2/CO_2; (c) Pt–Al_2O_3 catalysts coked by phenol.

bell-shaped signals culminated near 250°C. The burn-off temperature window for the deposits was unaffected by catalyst Pt-promotion. In addition, no additional distinctive peaks emerged in the CO_2 profile of Fig. 4b. Hence during combustion, there is no peak that could be assigned to Pt-catalyzed oxidation of carbons interacting with the metallic function.

The observed low-temperature combustion peaks suggest the importance of a transition metal oxide mediated burn-off route. This route is explained by the abundance, over the partially deactivated catalysts, of surface manganese oxide and of ceria, a well-known oxygen storage promoter [32]. A confirmation of availability, over spent catalysts, of accessible Mn and Ce oxides is provided by the XPS measurements, as shown in Fig. 5, in terms of percentage of abundance of atomic Mn and Ce for different CWO temperatures and constant oxidation time, t_{OX}.

The carbon content and the O_2 uptake for the spent MnO_2/CeO_2 exceeded those for the Pt-promoted MnO_2/CeO_2 (Table 1). It is inferred that catalyst promotion with platinum curbed deposition of the carbonaceous materials during the phase of *phenol conversion* so that less oxygen was required to burn-off the Pt–MnO_2/CeO_2 organic overlayer.

Shape and width invariance of the CO_2 evolution distributions as well as inhibition of the deposits by Pt are indeed plausible indicators that it was in the CWO phase, i.e. not during combustion, that platinum altered the structure of the polymeric deposits. During the TPO phase, the combustion mechanisms for both

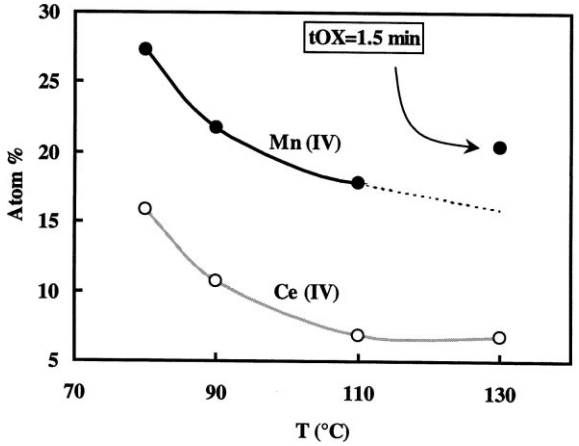

Fig. 5. XPS measurements of atomic surface composition of Mn and Ce for spent ceria-containing catalysts at CWO temperatures in the range (80–130°C) and $t_{OX} = 5$ min (percentage of Mn and Ce at 130°C extrapolated).

Table 1
Catalyst characteristics and CWO operating parameters

Catalyst	CWO temperature (°C)	Reaction time, t_{OX} (min)	TC on catalyst (μmol/(g cat.))	O_2 uptake in TPO (μmol/(g cat.))
Pt/Al_2O_3 fresh	–	–	0	0
Pt/Al_2O_3	175	60	3080	2430
Pt/Al_2O_3	175	240	4670	3010
MnO_2/CeO_2 fresh	–	–	0	310
MnO_2/CeO_2	80	15	920	910
MnO_2/CeO_2	80	120	5830	4450
$Pt–MnO_2/CeO_2$ fresh	–	–	0	250
$Pt–MnO_2/CeO_2$	80	15	830	860
$Pt–MnO_2/CeO_2$	80	90	4170	2730

spent catalysts are considered similar. This will be confirmed later by the comparable values of activation energy, pre-exponential frequency factor and oxygen partial order for the TPO of these catalysts.

Assuming further that the Gaussian peak distribution holds for the Pt/alumina catalyst, then the CO_2 profile can be fit using *one single* peak in Fig. 4c. This peak occurred at high temperature near 430°C and is typical for oxidation of carbons located on the metal oxide support [6]. Hence, it is very unlikely that the Pt-catalyzed carbon oxidation took place, since this step usually occurs at much lower temperatures around 200°C as reported by other investigators [6]. This finding further strengthens the above statement that platinum does not catalyze combustion of CWO deposits during TPO.

4.2.2. Pt inertness in burning off carbon

Two plausible reasons can most adequately explain the lack in activity of Pt while the deposits over $Pt–MnO_2/CeO_2$ or Pt/Al_2O_3 are being burnt off.

Hindrance effect: During phenol conversion, the metallic sites were progressively engulfed underneath the developing overlayer on the catalyst surface. These sites being buried and no longer accessible cannot catalyze C (nor H) combustion during TPO. Such mere geometrical interpretation is consistent with the declining Pt surface atom fraction as measured from XPS survey scans for spent Pt/Al_2O_3 and $Pt–MnO_2/CeO_2$ while phenol conversion was in progress.

Overoxidation deactivation: Deactivation by overoxidation of Pt could be another cause why Pt did not catalyze the TPO processes [33]. Calcination of the fresh catalysts and their subsequent exposure to oxidative environments both under CWO and TPO conditions obviously precluded the occurrence of metallic Pt. The detailed high-resolution Pt $4d_{5/2}$ region spectrum (Fig. 6a) for the spent Pt/alumina revealed indeed a binding energy of 315.5 eV typical of PtO [27,29,34,35]. On the other hand, the Pt $4f_{7/2}$ XPS line for the spent $Pt–MnO_2/CeO_2$ catalyst (Fig. 6b) corresponded to two doublets at 73.5 and 75.2 eV which can be assigned to PtO and PtO_2 [36], respectively. In both cases, no surface metallic Pt was detected by XPS.

4.2.3. Oxygen rate profiles

The oxygen consumption rate mirrored almost perfectly the CO_2 production rate (Fig. 4a–c). Furthermore, as can be seen in Table 1, the number of moles of O_2 consumed was seldom greater than the number of moles of CO_2 produced. This result, although counter-intuitive, is easily explained since the deposits themselves were already oxygenated due to the CWO reaction of phenol in the slurry reactor. It was indeed shown previously by means of XPS and static SIMS [28] that up to 25% of the surface carbon atoms were bearing oxygen. This "bound" oxygen contributed thus to oxidize hydrogen and carbon in the carbonaceous layer. In view of the discussion from the previous paragraph, it was unlikely that oxygen was further consumed by Pt. Furthermore, the Mn 2p and the Ce 3d XPS line spectra remained unshifted at BE = 641.9 and 882.6 eV, respectively, for all spent and fresh ceria-containing catalysts analyzed in this study. These values corresponded to invariable +4 oxidation states for cerium and manganese [28].

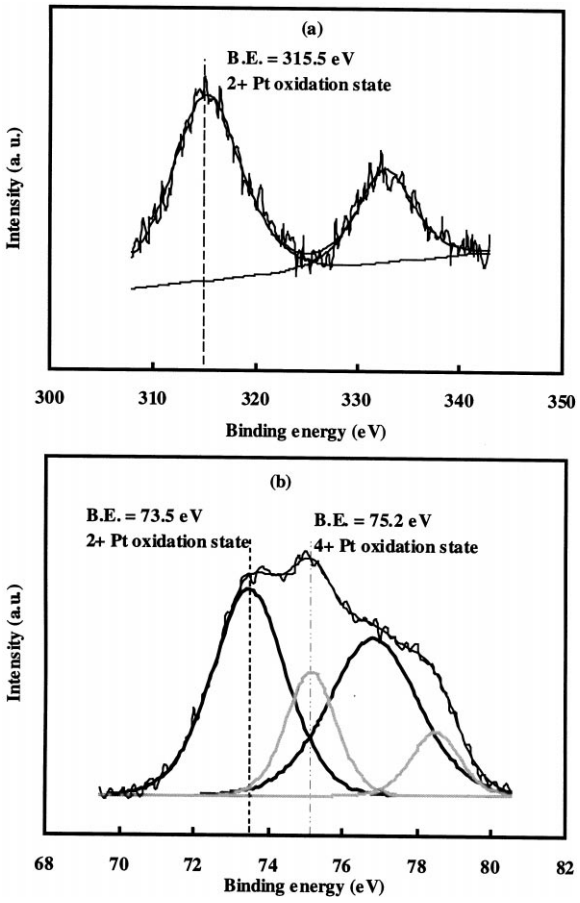

Fig. 6. (a) Spent Pt/Al_2O_3 catalyst: Pt $4d_{5/2}$ XPS high-resolution spectrum. (b) Spent $Pt–MnO_2/CeO_2$ catalyst: Pt $4f_{7/2}$ XPS high-resolution spectrum.

4.2.4. Water rate profiles

Water rate profiles exhibited much more complex shapes depending on the catalyst (Fig. 4a–c). The poor signal-to-noise ratios of the water MS signals of Fig. 4a and c indicate that the carbonaceous deposits over Pt/alumina and MnO_2/CeO_2 were poorly hydrogenated.

For the unpromoted ceria-based catalyst, the maximum water production rate occurred long after the CO_2 production was initiated. Detectable water fluxes persisted beyond the temperatures when CO_2 was no longer evolving (Fig. 4a). This might be ascribed to possible artifactual delays by H_2O re-adsorption on the non-heated tubes carrying the off-gases from the reactor to the MS. The TPO of the $Pt–MnO_2/CeO_2$ catalyst seems, however, not to support this scenario (Fig. 4b). On the contrary, it suggests that the dynamics of H_2O evolutions is characteristic of the combustibility of the deposits which may depend on the nature of the catalyst. Moreover, the coke overlayer on the $Pt–MnO_2/CeO_2$ was definitely the most hydrogenated.

Consistent with the above discussions, differences in the water evolution kinetics may be ascribed to variations in the deposit structure and probably not to different combustion mechanisms. Hence the presence of Pt on ceria-containing catalysts affects the incipient deposits only during phenol conversion in the CWO phase by promoting the formation of much hydrogenated coke laydown.

4.2.5. H/C ratio in the carbonaceous deposits

Temperature dependent H/C ratios are plotted in Fig. 7 for the runs depicted by Fig. 4a–c. These ratios, computed from $2 \times \mathrm{Rate}_{H_2O}/\mathrm{Rate}_{CO_2}$, can be interpreted only over the temperature range where both H_2O and CO_2 were detected meaningfully. By meaningful detection, it is meant only over a range where their proportions were reasonable. The high H/C ratios, up to 2.5 in the case of the $Pt–MnO_2/CeO_2$ deposit, was indeed an indication of hydrogen-rich deposits and also of the larger rates of hydrogen combustion with respect to that of carbon. Interestingly, these ratios were greater than the H/C ratio in phenol, i.e. $H/C = 1$.

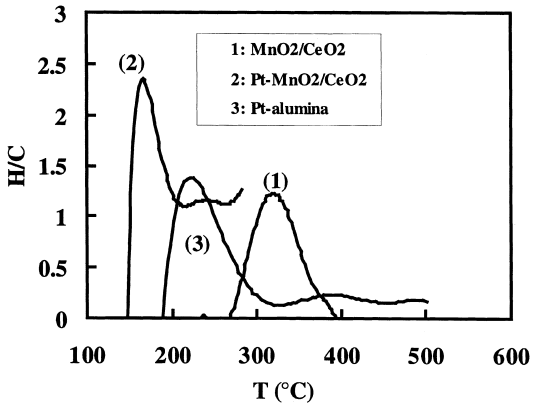

Fig. 7. Temperature-dependent H/C ratio for the spent: (1) MnO_2/CO_2; (2) $Pt–MnO_2/CO_2$; (3) $Pt–Al_2O_3$ catalysts coked by phenol in the CWO of Fig. 4.

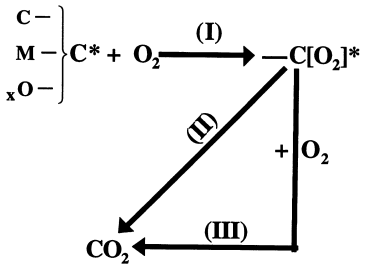

Fig. 8. Proposed combustion scheme of carbon occurring in CWO carbonaceous layers as observed by TPO.

5. Combustion pathway

A plausible fundamental mechanistic pathway underlying the combustion features of carbon according to the previous TPO observations could be as sketched in Fig. 8. This scheme is an offshoot of a mechanism recently proposed by Brown and coworkers [26,37] to describe the fate of burnt carbon during the TPO of cokes building up on cracking catalysts. As proposed here, it stipulates that a free carbon site, $-C^*$, in the form of carbon–carbon, carbon–metal or carbon–oxygen is available for O_2 chemisorption to form an undissociated dioxygen oxide $-C[O_2]^*$. The formation of dissociated surface oxides $-C[O]^*$ is very unlikely since no carbon monoxide was detected in the present study. Hence, the first step involves the adsorption of molecular oxygen onto a carbon of the carbonaceous overlayer to form a relatively stable oxygen-bearing surface complex. This step is followed by the desorption of undissociated oxide species $-C[O_2]^*$ leading to CO_2 (step II). An alternative route may also contribute to the heterogeneous elimination of CO_2 in which the complex of step I combines with oxygen via step III. From this proposed scheme, it can be expected that the overall combustion reaction order with respect to oxygen will be 1 when steps I and/or III are rate-determining. On the contrary, a zero-order dependence means that step II is the slowest. An order between 0 and 1 for O_2 would hence indicate that all three steps are competing.

6. Kinetic model for carbon dioxide evolution

An overwhelming amount of literature regarding the combustion kinetics of amorphous carbon, coal (pyrolyzed) coal- and wood chars [30,37] has been generated in studies on the burn-off kinetics of coke formed on cracking, reforming and selective hydrogenation catalysts [24–26]. Unfortunately, concerning quantitative approaches to the combustion kinetics of carbonaceous materials deposited during wet oxidation, not even a *single study* is available in the open literature.

By analogy, it is postulated thus that the quantitative phenomenological approach for char combustion [30] is also true for the combustion of CWO coke. Hence, the combustion pathway depicted in Fig. 8 will be modeled using the following general rate equation:

$$R = k_o \exp\left(-\frac{E}{RT}\right)[O_2]^m \ell(X) \tag{3}$$

where the last term, $\ell(X)$, can be thought of as a relative change in available carbon or surface area during coke combustion. From purely geometrical considerations and as suggested earlier by the BET specific surface areas, this function describes the departure of the pore surface area from the initial one as a function of coke conversion. This conversion is approximated by the conversion X of the residual carbon defined as

$$X(t) = 1 - \frac{[C(t)]}{[C]_o} \tag{4}$$

in which $[C]_o$ is the concentration, in μmol/(g cat.), of total carbon measured by elemental analysis, and $[C]$ the instantaneous residual carbon after a certain time t. It was derived by conversion of the MS signals into μmol/(g cat.) (see Eqs. (1) and (2)).

Recasting Eq. (3) for the non-isothermal coke burning in TPO experiments by introducing the carbon conversion, X, and the heating rate, β, gives

$$\frac{dX}{dT} = \frac{\tilde{k}_o}{\beta[C]_o} \exp\left(-\frac{E}{RT}\right)[O_2]^m \ell(X) \tag{5}$$

Application of Eq. (5) to our data rests on proposing an expression for the surface function $\ell(X)$. To accomplish this task two equivalent ways may be advocated. The first uses the Langmuir–Hinshelwood framework wherein the species intervening in Fig. 8 pathway are viewed as adsorbed/desorbed reactants and products [7,24,26]. This approach camouflages the landscape topology of the surfaces to be burnt into rate and adsorption equilibrium constants. The second approach

Table 2
Pore models tested against present TPO measurements

Grain model [Ref.]	$\ell(X)$	Parameters
Power-law [39], volume-reaction model [38], homogeneous model [30]	$(1-X)^n$	n: no physical meaning
Fractal power-law (this work)	$(1-X)^{D/3}$	D: fractal dimension of catalyst BET surface area
Structural non-overlapping [38]	$\dfrac{(1-X)^n}{1+[\sigma/(2n-1)][(1-X)^{1-n}-(1-X)^n(1+(Z-1)X^{1-2n})]}$	Z: Pilling–Bedworth ratio; σ: function of surface rate constant, grain initial area, product layer diffusivity, porosity
	$\dfrac{\sqrt{1-X}}{1+\sigma\sqrt{1-X}[\ln(1-(Z-1)X)-\ln(1-X)]}$ if $n=\frac{1}{2}$	
Pore tree [40]	$(1-X)\sqrt{1-X+X\varepsilon_o^{-1}}$	ε_o: initial porosity
Random pore [41]	$(1-X)\sqrt{1-\phi\ln(1-X)}$	f: structural parameter
Random capillary [42]	$(1-X)\sqrt{1-\dfrac{B_o\ln(1-X)}{2\pi B_1^2}}$	B_o/B_1: pore length (surface) constants
Bifurcated pore [43]	$(1-X)\sqrt{1+\dfrac{\ln(1-X)}{\ln(1-\varepsilon_\mu)}}$	ε_μ: initial micro-pore porosity
Semi-empirical structural [44]	$\lambda(1-X)\sqrt{X}$	λ: adjusted constant

uses pore models [30] or volume-reaction (or homogeneous) models [38] for $\ell(X)$, and will be adopted in the following development.

A summary of the various $\ell(X)$ pore model expressions is provided in Table 2. An overview of these models and their accuracy in predicting kinetic data is discussed in detail in [30,38]. Among these pore models, the power-law grain model is probably the simplest one.

The pore models, presented in Table 2, were fitted to the TPO data of MnO_2/CeO_2 spent catalyst coke combustion as depicted in Fig. 9. Values of the pre-exponential factor $\tilde{k}_o$, the activation energy, E and the partial order with respect to oxygen, m were identified. Parameter identification was performed by means of an unconstrained optimization method using a mixed quadratic-cubic line search procedure (Matlab® Software from MathWorks). The goodness-of-fit of these models was assessed by the minimization of the objective function of the residuals (or variance) between measured, X_i, and predicted, $\hat{X}_i$ (integrated), CO_2 conversion data:

$$\sigma^2 = \frac{1}{N_{\text{data}}}\sum_i (X_i - \hat{X}_i)^2 \tag{6}$$

From Table 3 and Fig. 9, it can be seen that the much simpler four-parameter power-law grain model performed better than the rest of the pore models so that no substantial gain was attained using them on our experimental kinetic data. The same parameters (E, $\tilde{k}_o$ and m) were obtained for the pore tree, the random pore, the random capillary and the bifurcated pore models, whereas the power-law grain model predicted higher activation energy and oxygen partial order. The power-law grain model suggests that steps I and III in the combustion pathway (Fig. 8) are rate-controlling as the oxygen order m was unity. The fitted m order for the other pore models, on the contrary, predict that step II retardation is not marginal.

The simplicity and accuracy of the power-law grain (or homogeneous) model justify its subsequent use for

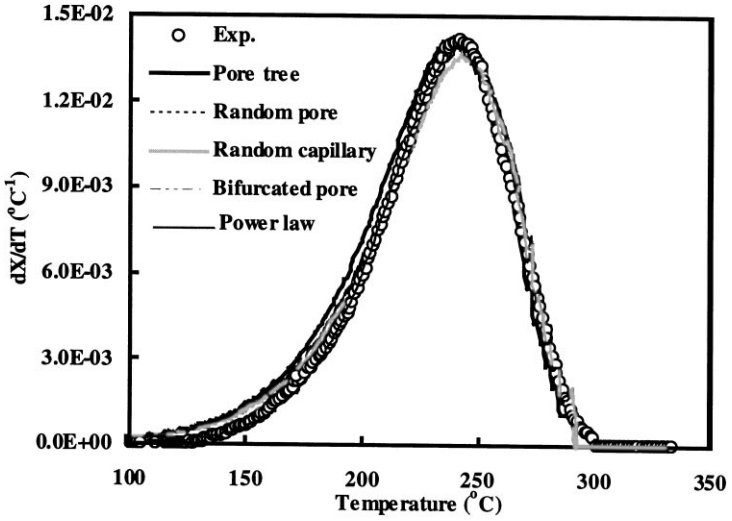

Fig. 9. Experimental versus simulated CO_2 conversion profiles with various structural pore models. Coke formed on MnO_2/CeO_2 catalyst. CWO conditions: $T = 80^\circ C$, $t_{OX} = 15\,min$, $P_{O_2} = 0.5\,MPa$.

all spent catalysts studied in this work. Usually, the parameter n has been assigned no physical meaning. From geometrical considerations (see Appendix A), the values of the fractal dimension measured previously can be used instead of the parameter n. Identifying n to $\frac{1}{3}D$ highlights a relation between the coke reactivity to combustion and the topology of the spent catalyst surface. Under these circumstances, the number of adjustable parameters in the power-law grain model reduces to three, i.e., E, $\tilde{k}_o$ and m, and Eq. (5) becomes

$$\frac{dX}{dT} = \frac{\tilde{k}_o}{\beta[C]} \exp\left(-\frac{E}{RT}\right)[O_2]^m (1-X)^{D/3} \qquad (7)$$

Optimized parameters required to represent by Eq. (7) evolved CO_2 during TPO of CWO coke deposited on the spent MnO_2/CeO_2, Pt–MnO_2/CeO_2 and Pt–Al_2O_3 are listed in Table 4. Fig. 10a–d illustrate the fit to the TPO of the catalysts aged under the CWO oxidations summarized in Table 4.

The most meaningful data quoted in Table 4 are the oxygen partial order and the activation energy. Comparison of the rate constant parameters, that is activation energy and pre-exponential frequency factor, are consistent with the compensation effect [26]. For example, the coke formed over Pt–Al_2O_3 after 60 min aging exhibited low activation energy and low pre-exponential factor compared to that aged for 240 min. The higher activation energy and pre-exponential factor in the latter case indicate that the deposited coke was more difficult to oxidize and required a higher temperature range to undergo complete combustion (see also Fig. 10c and d).

Table 3
Comparison of six literature models for "coke" combustion over MnO_2/CeO_2 spent catalyst[a]

Model	E (kJ/mol)	$\tilde{k}_o$	m	Model parameter	Error
Power-law'	71.6	8.0×10^4	1.0	$n = 0.97$	35×10^{-2}
Pore tree	53.4	5.8×10^6	0.24	$\varepsilon_o = 0.24$	103×10^{-2}
Random pore	53.4	5.8×10^6	0.22	$\phi = 2.9$	66×10^{-2}
Random capillary	53.4	5.8×10^6	0.22	$B_o = 1.37$, $B_1 = 0.27$	66×10^{-2}
Bifurcated pore	53.4	5.8×10^6	0.22	$\varepsilon_\mu = 0.33$	73×10^{-2}
Semi-empirical structure	48.9	6.1×10^6	0.36		63×10^{-2}

[a] Phenol CWO: $t_{OX} = 15\,min$, $P_{O_2} = 0.5\,MPa$, $T = 80^\circ C$.

Table 4
Optimized rate coefficient parameters and O_2 reaction orders for the fractal power-law grain model for the different spent CWO catalysts

Catalyst	CWO temperature (°C)	P_{O_2} (MPa)	t_{OX} (min)	E (kJ/mol)	$\tilde{k}_o$	m	$\frac{1}{3}D$
MnO_2/CeO_2 (Fig. 10a)	80	0.5	15	72	5.8×10^6	0.80	0.85
$Pt–MnO_2/CeO_2$ (Fig. 10b)	80	0.5	15	84	5.8×10^6	1.0	0.84
Pt/Al_2O_3 (Fig. 10c)	175	1.5	60	53	7.9×10^4	0.44	0.78
Pt/Al_2O_3 (Fig. 10d)	175	1.5	240	88	8.8×10^6	1.0	0.82

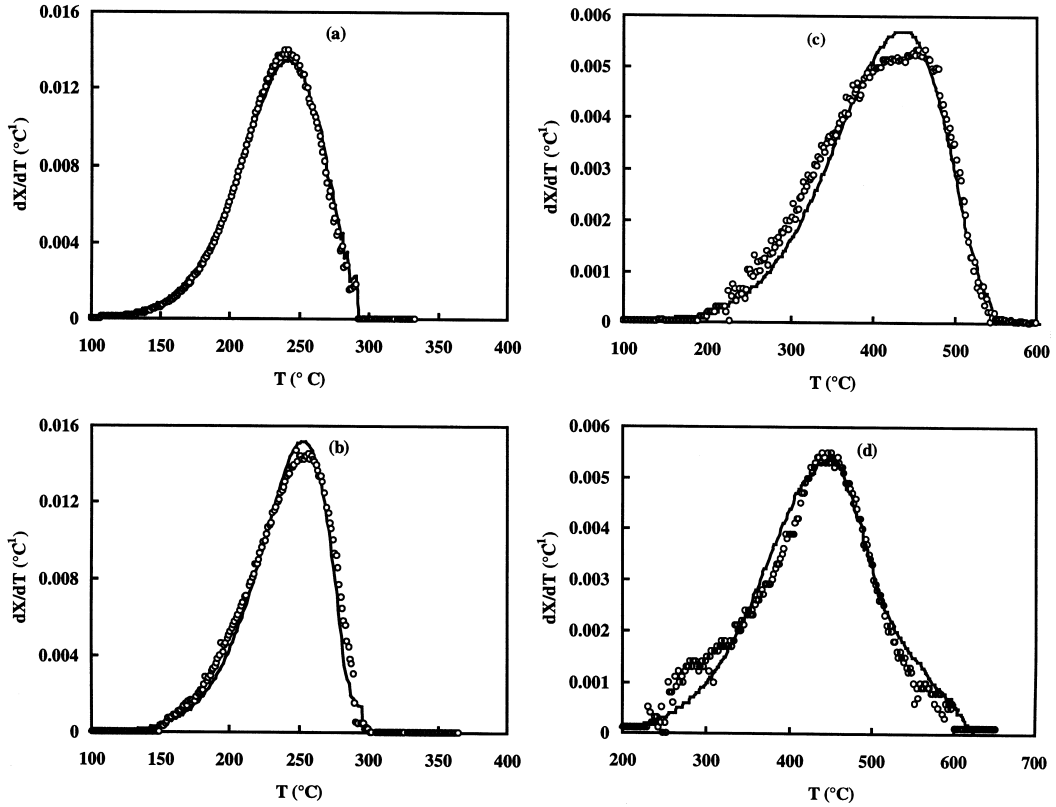

Fig. 10. Measured and simulated CO_2 conversion evolution rates during TPO of spent: (a) MnO_2/CO_2; (b) $Pt–MnO_2/CO_2$; (c) and (d) $Pt–Al_2O_3$ catalyst.

As speculated earlier (Fig. 8), the oxygen partial order m lies in the range (0–1) [30,45–47]. For Pt–alumina, m increased from 0.44 to 1.0 when the CWO exposure was increased from 60 to 240 min. This might indicate that the combustion mechanism of Fig. 8 changed from a mixed-control at low CWO exposure times ($t_{OX} = 60$ min) to I–III step control at high CWO exposure times ($t_{OX} = 240$ min).

Interestingly, the cokes deposited over $Pt–MnO_2/CeO_2$ and MnO_2/CeO_2 catalysts under the same CWO conditions of exposure, temperature and oxygen pressure were characterized by very close kinetic TPO parameters, i.e. oxygen partial order, pre-exponential factor and activation energy. These results are not surprising and agree well with the interpretations provided in Section 4.2.1.

7. Conclusion

The burn-off kinetics of three spent wet oxidation catalysts, “coked” with phenol in a slurry reactor, were

measured, interpreted and modeled using a modified fractal power-law grain model.

Interpretation of the observed TPO evolution rates of water, oxygen and carbon dioxide led to the following conclusions:

1. For the Pt-doped catalysts, the noble metal did not catalyze the burn-off of the carbonaceous materials.
2. The absence of carbon monoxide in the combustion gases suggested that the heterogeneous elimination of CO_2 resulted from two reaction steps, the desorption and/or the interaction with oxygen of an undissociated dioxygen-bearing surface carbon species.
3. The severity of the CWO appeared to have an impact on the kinetic parameters of the CO_2 burn-off profiles. Low-severity cokes on Pt/alumina burnt via a combustion mechanism with two controlling steps (oxygen partial order $= 0.44$). The high severity cokes burn-off was not limited by the physical desorption of the undissociated dioxygen intermediate species (oxygen partial order $= 1.0$).
4. The activation energies and oxygen partial orders for the low-severity coke over Pt-promoted and unpromoted ceria-containing spent catalysts did not differ by more than 20%. This might suggest that the deposits obeyed identical combustion mechanisms where physical desorption of the undissociated dioxygen intermediate species was fast.

Acknowledgements

Financial support from the Natural Sciences and Engineering Research Council of Canada (NSERC) and the Fonds pour la Formation de Chercheurs et d'Aide à la Recherche (Québec) is gratefully acknowledged. The authors thank Prof. B. Grandjean for the mass spectrometer and Dr. M. Cassanello (Universidad de Buenos Aires, Argentina) for taking the SEM and nitrogen adsorption measurements.

Appendix A. Expression of $\ell(X)$ as a function of the fractal dimension D

We assume that the (coke + catalyst) assemblage looks like spheroids of characteristic length ξ. We further assume that the spheroid size shrinks "topochemically" as combustion evolves so that its geometrical parameters are preserved. Since the spheroid surface is fractal, with fractal dimension D, we can write

$$S = \psi_A \xi^D \tag{A.1}$$

$$V = \psi_V \xi^3 \tag{A.2}$$

in which ψ_A and ψ_V are area and volume shape factors, respectively.

Assuming that the coke density is constant during the course of combustion and that mass conversion of the carbonaceous material is equal to the carbon conversion X, we have the following proportionality:

$$\xi \equiv \sqrt[3]{1 - X} \tag{A.3}$$

As said previously, $\ell(X)$, is a measure of the relative change in available surface area. This function describes the departure of the pore surface area from the initial one [30] as a function of coke conversion. We have thus

$$\ell(X) \equiv S \equiv (1 - X)^{D/3} \tag{A.4}$$

Replacing in Eq. (7), $\ell(X)$ by Eq. (A.4) gives

$$\frac{dX}{dT} = \frac{\tilde{k}_o}{\beta[C]} \exp\left(-\frac{E}{RT}\right) [O_2]^m (1 - X)^{D/3} \tag{A.5}$$

References

[1] Y.I. Matatov-Meytal, M. Sheintuch, Ind. Eng. Chem. Res. 37 (1998) 309.
[2] A. Pintar, J. Levec, J. Catal. 135 (1992) 345.
[3] S. Hocevar, J. Batista, J. Levec, J. Catal. 184 (1999) 39.
[4] S. Hamoudi, F. Larachi, G. Cerella, M. Cassanello, Ind. Eng. Chem. Res. 37 (1998) 3561.
[5] S. Hamoudi, K. Belkacemi, F. Larachi, Chem. Eng. Sci. 54 (1999) 3569.
[6] S.M. Augustine, G.N. Alameddin, W.M.H. Sachtler, J. Catal. 115 (1989) 217.
[7] C. Li, T.C. Brown, Energy and Fuels 13 (1999) 888.
[8] F.E. Massoth, Ind. Eng. Chem. Process. Des. Dev. 6 (1967) 200.
[9] A. Brito, R. Arvelo, F.J. Garcia, A.R. Gonzalez, Appl. Catal. A 145 (1996) 285.
[10] C.N. Satterfield, T.K. Sherwood, The Role of Diffusion in Catalysis, Addison-Wesley, Reading, MA, 1963.
[11] B.S. Sampath, P.A. Ramachandran, R. Hughes, Trans. Inst. Chem. Eng. 53 (1975) 53.
[12] B.S. Sampath, P.A. Ramachandran, R. Hughes, Chem. Eng. Sci. 30 (1975) 125.

[13] V.R. Shettigar, V. Venkateswaran, Chem. Eng. J. 16 (1978) 165.
[14] S.V. Sotirchos, E. Mon, N.R. Amundson, Chem. Eng. Sci. 38 (1983) 55.
[15] J.J. Carberry, in: Chemical and Catalytic Reaction Engineering, McGraw-Hill, New York, 1976, p. 310 (Chapter 7).
[16] O. Levenspiel, in: Chemical Reaction Engineering, Wiley, New York, 1999, p. 566.
[17] G. Wang, S. Lin, W. Mo, G. Peng, G. Yang, Ind. Eng. Chem. Process. Des. Dev. 25 (1986) 626.
[18] C.L. Pieck, R.L. Verderone, E.L. Jablonski, J.M. Parera, Appl. Catal. 55 (1989) 1.
[19] C. Royo, M. Menéndez, J. Santamaría, React. Kinet. Catal. Lett. 44 (1991) 445.
[20] J.M. Ortega, A.G. Gayubo, A.T. Aguayo, P.L. Benito, J. Bilbao, Ind. Eng. Chem. Res. 36 (1997) 60.
[21] V.D. Dimitriadis, A.A. Lappas, I.A. Vasalos, Fuel 77 (1998) 1377.
[22] J.M. Arandes, I. Abajo, I. Fernández, D. López, J. Bilbao, Ind. Eng. Chem. Res. 38 (1999) 3255.
[23] A.T. Aguayo, A.G. Gayubo, A. Atutxa, M. Olazar, J. Bilbao, J. Chem. Technol. Biotechnol. 74 (1999) 1082.
[24] C.A. Querini, S.C. Fung, Appl. Catal. A 117 (1994) 53.
[25] M. Larsson, J. Jansson, S.J. Asplund, J. Catal. 178 (1998) 49.
[26] C. Li, C. Le Minh, T.C. Brown, J. Catal. 178 (1998) 275.
[27] S. Hamoudi, F. Larachi, A. Sayari, J. Catal. 177 (1998) 247.
[28] S. Hamoudi, F. Larachi, A. Adnot, A. Sayari, J. Catal. 185 (1999) 333.
[29] J.A. Rossin, J. Mol. Catal. 58 (1990) 363.
[30] A.M.C. Janse, H.G. De Jonge, W. Prins, W.P.M. van Swaaij, Ind. Eng. Chem. Res. 37 (1998) 3909.
[31] R.J. Aguerre, P.E. Viollaz, C. Suárez, Lebensmittel-Wissenschaft und-Technologie 30 (1996) 227.
[32] A. Trovarelli, Catal. Rev. Sci. Eng. 38 (1996) 439.
[33] J.H. Vleeming, B.F.M. Kuster, G.B. Marin, Ind. Eng. Chem. Res. 36 (1997) 3541.
[34] J.Z. Shyu, K. Otto, Appl. Surf. Sci. 32 (1988) 546.
[35] J.C. Vedrine, M. Dufaux, C. Naccache, B. Imelik, J. Chem. Soc., Faraday Trans. 74 (1978) 440.
[36] C.D. Wagner, in: D. Briggs, M.P. Seah (Eds.), Practical Surface Analysis, Vol. 1, 2nd Edition, Wiley, Chichester, UK, 1990, p. 621.
[37] C. Le Minh, R.A. Jones, I.E. Craven, T.C. Brown, Energy and Fuels 11 (1997) 463.
[38] S.K. Bhatia, J.S. Gupta, Rev. Chem. Eng. 8 (1992) 177.
[39] A. Kritiansen, Understanding Coal Gasification, IEA Coal Research, London, 1995.
[40] G.A. Simons, M.L. Finson, Combust. Sci. Technol. 19 (1979) 217.
[41] S.K. Bhatia, D.D. Perlmutter, AIChE J. 26 (1980) 379.
[42] G.R. Gavalas, AIChE J. 26 (1980) 577.
[43] H.P. Tseng, T.F. Edgar, Fuel 68 (1989) 114.
[44] E. Chornet, J.M. Baldasano, H.T. Tarki, Fuel 58 (1979) 395.
[45] N.M. Laurendeau, Prog. Energy Sci. 4 (1978) 221.
[46] L.C. Lin, M.D. Deo, F.V. Hanson, A.G. Oblad, Ind. Eng. Chem. Res. 30 (1991) 1795.
[47] M. Larsson, Coke on supported palladium and platinum catalysts, Ph.D. Thesis, Chalmers University, Göteberg, Sweden, 1997.